ELSEVIER

Journal of Fluids and Structures 22 (2006) 1113–1131

JOURNAL OF FLUIDS AND STRUCTURES

www.elsevier.com/locate/jfs

# Simulation of cross-flow-induced vibration of cylinder arrays by surface vorticity method

K. Lam[a,*], G.D. Jiang[b], Y. Liu[a], R.M.C. So[a]

[a]*Department of Mechanical Engineering, The Hong Kong Polytechnic University, Hung Hom, Kowloon, Hong Kong, PR China*
[b]*School of Mechanical Engineering, Xi'an Jiaotong University, Xi'an, PR China*

Received 25 May 2004; accepted 13 March 2006
Available online 27 July 2006

**Abstract**

The surface vorticity method (SVM), which is a fast and practical grid-free two-dimensional (2-D) method, and a fluid–structure interaction model incorporating the effects of cylinder motions and displacements is used to simulate the vortex-induced vibration of cylinder arrays at sub-critical Reynolds number $\mathrm{Re} = 2.67 \times 10^4$. The SVM is found to be most suitable for simulating a 2-D cylinder row with large-amplitude vibrations where the vorticity field and the fluid forces of the cylinder row change drastically, and the effect of the stream on the transverse direction vibration is very significant. The fluidelastic instability of a flexible cylinder row at small pitch ratio is also investigated, and the critical reduced velocity of the cylinder row at a reduced damping parameter $S_G = 1.29$ is calculated, which is in good agreement with experimental and analytical results of the unsteady model. Vortex-induced vibration of a staggered cylinder array is simulated using different structural parameters. When the cylinders are relatively more flexible, the flow pattern changes dramatically and the fluid–structure interaction has a dominant impact on the flow field. Compared with grid-based methods, the grid-free SVM is a fast and practical method for the simulation of the FIV of cylinder arrays due to vortex shedding at sub-critical Reynolds numbers.


## 1. Introduction

It is well known that tube bundle failures due to cross-flow-induced vibrations may be a catastrophic event in heat exchangers and steam generators of nuclear power plants. During the past 30 years, considerable investigations have been carried out and reported in the open literature to explain the phenomenon of flow-induced vibration failure; some design guidelines have also been proposed. Excellent reviews are given by Païdoussis (1983), Weaver and Fiztpatrick (1988), Moretti (1993), Blevins (1994), Price (1995), and Pettigrew and Taylor (2003a, b). It is generally accepted that there are four vibration excitation mechanisms in flow-induced vibrations (FIV) of tube bundles. They are: (a) fluidelastic instability; (b) vortex shedding excitation; (c) turbulence buffeting; and (d) acoustic excitation. Fluidelastic instability is the most important mechanism. It is the result of fluid–structure interaction and reflects the unsteady nature of the interstitial flow in the tube bundle. A number of theoretical models have been used to analyse the fluidelastic instability (Price, 1995). Some of the more notable ones are: (i) the jet-switch model; (ii) quasi-static models; (iii) inviscid flow models; (iv) unsteady models; (v) semi-analytical models; (vi) quasi-steady models; and

*Corresponding author. Tel.: +852 2766 6649; fax: +852 2365 4703.
*E-mail address:* mmklam@polyu.edu.hk (K. Lam).

0889-9746/$ - see front matter © 2006 Elsevier Ltd. All rights reserved.
doi:10.1016/j.jfluidstructs.2006.03.004

(vii) computational fluid dynamics (CFD) models. Among the conventional semi-empirical prediction methods, the unsteady model used by Tanaka et al. (2002) and Chen and Srikantiah (2002) is among the most successful models. However, this model is based on experimental unsteady fluidelastic force coefficient data, which is difficult to obtain and up to the present, is only available for some types of tube bundle configurations and several pitch ratios $P/D$. On the other hand, CFD models have the potential of being less expensive and more accurate in simulating the real flow situation, and can be used for any arbitrary tube bundle configurations. In addition, flow field data, such as vorticity contours, streamlines, fluid forces, velocity contours, and tube dynamics data can be obtained at each time step.

With the advent of computers and computational methods, CFD research on flow-induced vibration of tube bundles has been carried out in the past couple of decades. Ichioka et al. (1994) simulated the flow-induced vibrations of a row of cylinders using finite difference method (FDM) to solve the Navier–Stokes (N–S) equations at different Reynolds numbers (Re). The time history waveform of cylinder displacements and the critical reduced velocity for instability at $T/D = 1.35$ and two different structural parameters was presented and compared with experiment results. Kassera and Strohmeier (1997) calculated the flow-induced vibrations of six flexible tube bundles using a finite volume method (FVM) to solve the Reynolds equations with a $k$–$\omega$ turbulence model. The tube displacement root mean square (r.m.s.) values at different reduced velocities were presented together with the measured results. Schroder and Gelbe (1999) simulated the fluid–structure coupling of a flexible tube row and a fully flexible tube bundle by the FVM with different turbulence models. In their paper, the fluidelastic instability for a tube row, and the pressure distribution and fluidelastic instability for a three-row tube bundle were given and compared with experimental results. Longatte et al. (2003) calculated the cross-flow-induced vibrations of a flexible tube in an in-line fixed tube bundle by FVM and using a unit cell computational domain with symmetrical boundary hypothesis. The tube vibration frequency at small flow velocity was presented.

Due to the large number of meshes needed for multi-tube simulation and the time-consuming mesh redistribution requirement for tube vibration, almost all the above computations have to be conducted on workstations or mini-supercomputers. Furthermore, the calculations were limited to small tube vibrations because of mesh constraints. When computational accuracy and costs also have to be considered, it can be said that up to the present, most FDM and FVM are impractical for flow-induced vibration simulation of large numbers of flexible tubes at practical Re. In general, the finite element method (FEM) is more appropriate for complex FIV and moving boundary problems compared to FDM, and the grid distributions used can be more flexible. However, FEM requires more computational time than FDM; therefore, up to the present, FEM simulation of flow-induced vibration of multi-cylinders is still limited to laminar flow and simple tube configurations.

Liu et al. (2001) computed the flow-induced vibration of two side-by-side circular cylinders using FEM at $\mathrm{Re} = 200$, and Mittal and Kumar (2001) calculated the flow-induced oscillation of a pair of cylinders in tandem and staggered arrangements using FEM at $\mathrm{Re} = 160$, while Kevlahan and Ghidaglia (2001) computed the turbulent flow past an array of cylinders using a spectral method with a Brinkman penalization fluid–structure interaction model. Seitanis and Anagnostopoulos (2000) investigated numerically the in-line oscillation of a two row tube bundle using FEM at $\mathrm{Re} = 200$. In their work, one row of cylinders is fixed while the other row of cylinders is allowed to move as a whole. The time history of the force coefficients and displacements, the streamlines and the vorticity contours over one oscillation cycle were presented. The FDM/FEM could also be used to tackle multi-cylinder FIV with large vibration amplitudes if a mesh-shape preservation technique is implemented to prevent mesh entanglement. Recently, So et al. (2003) have successfully applied this technique to simulate the FIV of two side-by-side cylinders with large vibration amplitude. In this paper, an attempt is made to use FEM and the mesh remapping technique to simulate fluidelastic instability of cylinder arrays at sub-critical Re, and the results are compared with the surface vorticity method (SVM) calculations.

Vortex methods have long been regarded as a natural and efficient approach for flow simulation. Readers can refer to Cottet and Koumoutsakos (2000) or Lewis (1991) for a detailed description of the vortex method. Such methods concentrate on simulating the vorticity field and directly capture the physical nature of the flow around bluff bodies. In particular, the grid-free approach is ideal for flow-induced vibration problems since the bodies can be allowed to move freely over a large distance without the limitation of the grid. Zhou et al. (1999) simulated the flow-induced vibration of an elastic cylinder using a discrete vortex method and vortex-in-cell technology. Shiels et al. (2001) numerically simulated the transverse oscillation of a dynamically supported circular cylinder in a flow at $\mathrm{Re} = 100$ using a high-resolution viscous-vortex method. Sweeney and Meskell (2003) conducted a fast numerical simulation of the vortex shedding in a normal triangular tube bundle using a discrete vortex method and a cloud-in-element technique. Although the introduction of the vortex-in-cell or cloud-in-element techniques provides substantial savings to computational time, it also makes the method grid-dependent to a certain extent. Based on a 2-D SVM, which is basically a variant of the deterministic vortex method, Lam et al. (2004) proposed a new vortex–structure interaction model to simulate the flow-induced vibration of multi-cylinders. The model incorporates vortex–cylinder interaction including the effects of

cylinder displacement and cylinder motion. With this computational approach, the flow-induced vibration of one and two flexible cylinders were successfully simulated at $\mathrm{Re} = 2.67 \times 10^4$, with a dimensionless time step $\Delta t\, U/D = 0.075$, and the cylinder responses, the fluid forces, the vibration frequencies, and the vorticity map were presented.

The objective of the present investigation is to apply this simple yet efficient method to study 2-D fluid–structure interaction of a large number of infinitely long tubes in a cross flow at sub-critical Re.

The computational methodology is briefly described first. The method is then applied to simulate the vortex-induced vibration and fluidelastic instability of a single row of seven cylinders at $\mathrm{Re} = 2.67 \times 10^4$. This can be regarded as one of the standard cases of cylinder arrays for fluidelastic instability analysis. The vorticity map, fluid force, vibration response, shedding frequency, and the critical reduced velocity of the centre tubes are compared with experimental results. Finally, the vortex-induced vibration of a three-row staggered cylinder array and a tube bundle with 14 cylinders is studied at similar Re and time step to gain insight into fluidelastic instability of more complex situations. It should be noted that this model does not simulate turbulent buffeting or acoustic resonance, which are also major causes for flow-induced vibration.

## 2. Formulation of vortex-induced vibration simulation

In any fluid–structure interaction simulation problem, it is necessary to first calculate the flow field, then the structural dynamics and finally the fluid–structure interaction. Therefore, the SVM and a two-degree-of-freedom structural dynamics model for 2-D cylinder arrays are discussed first. Then, the fluid–structure interaction model, i.e. the coupling between the vorticity field and the flexible cylinders, is described.

### 2.1. Surface vorticity method (SVM)

The fluid motion is governed by the Navier–Stokes equations. For 2-D incompressible flow, the governing equations can be transformed to the vorticity transport equation, which is

$$\frac{\partial \omega}{\partial t} + \vec{V} \cdot \nabla \omega = \nu \nabla^2 \omega, \tag{1}$$

where $\omega$ is the vorticity, $\vec{V}$ is the velocity vector, $t$ is time, and $\nu$ is the fluid kinematic viscosity. According to (1), flow development can be regarded as vorticity generation (shedding), $\partial\omega/\partial t$, vorticity convection $\vec{V} \cdot \nabla \omega$, and vorticity diffusion $\nu \nabla^2 \omega$.

When a cross-flow passes a bluff body, a very thin boundary layer is developed. Due to the no-slip condition at the wall, the tangential velocity outside the boundary layer varies quickly to zero at the wall. In the Martensen's surface vorticity method, this thin boundary layer is simplified to a vorticity sheet of strength $\gamma(s)$ moving parallel to the surface of the body. In numerical simulations, this continuous vorticity sheet is discretized to a number of surface vorticity elements called surface vorticity. By circulation considerations with the no-slip condition at the wall, the strength of the surface vorticity is equal to the surface-free-stream velocity just outside boundary layer. For convenience, the tangential surface velocity just outside the boundary layer is called the "surface velocity" $u_s$ in this paper. Therefore, we have $\gamma(s) = u_s$ and the convection velocity of the vorticity sheet is at $u_s/2$. The strength of the surface vortex is calculated by Martensen's integral potential flow equation by applying Biot–Savart induction law between vortices. Lewis (1981, 1991) modified the integral equation by taking into account the additional coupling effects due to the free vortices for separated flow. As a result, the strength of the $m$th surface vortex element can be represented by

$$\sum_{n=1}^{M} \gamma(s_n) K(s_n, s_m) \Delta s_n = -U \left[ \frac{\mathrm{d}x_m}{\mathrm{d}s_m} \cos\alpha + \frac{\mathrm{d}y_m}{\mathrm{d}s_m} \sin\alpha \right] + \sum_{i=1}^{I} \Delta\Gamma_i L(i,m), \tag{2}$$

where $\gamma(s_n)$ is the $n$th surface vortex strength, $K(s_n, s_m)$ is the coupling coefficient of the $n$th surface vortex to the $m$th surface vortex, $\Delta s_n$ is the length of the $n$th surface vortex element, $U$ is the mainstream velocity, $\alpha$ is the angle between the $x$-direction and the mainstream direction, $\mathrm{d}x_m/\mathrm{d}s_m$ and $\mathrm{d}y_m/\mathrm{d}s_m$ are the projection factors of the $x$-direction and the $y$-direction to the surface tangent direction, respectively, $\Delta\Gamma_i$ is the vorticity of the $i$th free vortex, $L(i,m)$ is the coupling coefficient of the $i$th free vortex to the $m$th surface vortex element, $M$ is the total number of surface vortex, and $I$ is the total number of free vortices.

For separated flow simulation, at each time step, the separation points on the surface are determined by the velocity direction scheme (VDS) proposed by Lam et al. (2004). The surface vortices behind the separation point are shed from the surface at a small distance normal to the surface and become free vortices (Rankine vortices). The free vortices move

under the influence of the convection velocity, the surface vortices and other free vortices, and viscous diffusion of the free vortices. On the other hand, convection of the free vortices is governed by the Biot–Savart induction theorem (Lewis, 1991), and viscous diffusion of the free vortices is evaluated by the diffusion velocity method proposed by Ogami and Akamatsu (1991). The surface vortices are also affected by the moving free vortices, which account for an additional term in the Martensen's potential flow equation. Therefore, the vorticity distribution in the flow field can be determined. Once known, the velocity field can be calculated from the vorticity distribution.

### 2.2. Calculation of the force coefficients

The pressure distribution around the cylinder is calculated using the energy equation and the dynamic pressure loss across the free layer is accounted for using the method proposed by Lewis (1981). Thus formulated, the dimensionless static pressure coefficients can be written as

$$\begin{cases} C_p = C_{p0} - (u_s/U)^2, & \text{upstream of the separation point,} \\ C_p = C_{p0} - (u_s/U)^2 - (u_{sp}/U)^2, & \text{downstream of the separation point,} \end{cases} \tag{3}$$

where $C_p$ is the dimensionless pressure coefficient, $C_{p0}$ is the dimensionless stagnation point pressure coefficient, $u_s$ is the "surface velocity", and $u_{sp}$ is the "surface velocity" at the vortex element just before the separation point. At sub-critical Re, the effect of skin friction on the mean drag of a bluff body is negligibly small. Therefore, the lift and drag coefficient can be obtained by integrating the pressure coefficients around the bluff body, i.e.,

$$C_D = \frac{1}{2}\int_0^{2\pi} C_p \cos\theta \, \mathrm{d}\theta, \tag{4}$$

$$C_L = \frac{-1}{2}\int_0^{2\pi} C_p \sin\theta \, \mathrm{d}\theta, \tag{5}$$

where $\theta$ is the circumferential location of $C_p$.

### 2.3. Structural dynamics

In the present formulation, only the unsteady forces act on the cylinder along the $x$- and $y$-direction are considered. Assuming a two-degree-of-freedom (2-dof) model, the dynamical equation of the cylinder can be written in dimensionless form as

$$\ddot{\mathbf{Z}} + \frac{4\pi\zeta_S}{U_r}\dot{\mathbf{Z}} + \left(\frac{2\pi}{U_r}\right)^2 \mathbf{Z} = \frac{C_F}{2M}, \tag{6}$$

where $\mathbf{Z} = (X/D)\mathbf{i} + (Y/D)\mathbf{j}$, $X$ and $Y$ are the instantaneous displacement of the cylinder in the $x$ and $y$ direction, respectively, $D$ is the diameter of the cylinder, $\zeta_S = c/(2\sqrt{km})$ is the dimensionless structural damping coefficient, $c$ is the damping coefficient, $k$ is the equivalent stiffness, $m$ is the structure mass per unit length, $U_r = U/(f_N D)$ is the reduced velocity, $f_N$ is the natural frequency of the structure, $M = m/(\rho D^2)$ is the mass ratio, $C_F$ is the unsteady fluid force coefficient vector with components $C_D$ and $C_L$ along the $x$- and $y$-direction, respectively, and $\rho$ is the fluid density. The mean and root-mean-square parts of $C_D$ and $C_L$ are denoted as $\bar{C}_D$, $C'_D$ and $\bar{C}_L$, $C'_L$, respectively. These dynamic equations are solved using a fourth-order Runge–Kutta method. Once the equations are solved, the velocity of the cylinder and its displacements can be determined.

In order to show the effect of the structural dynamics model, a 1-dof vibration model will also be assumed in later calculations. In this 1-dof model, vibration only in the transverse direction is considered and the governing equation is given by setting $X$ to zero in Eq. (6). Thus, the 1-dof calculations can be compared with the 2-dof results to gain better understanding of the vibration behaviour of an elastic cylinder row. In particular, this allows the effect of crosstalk between the $x$- and $y$-direction vibrations to be investigated.

### 2.4. Fluid–structure interaction model

An inertial frame of reference is used to describe the flow field and all structures are vibrating relative to this reference frame. Lam et al. (2004) simulated the flow-induced vibration of a single flexible cylinder at $\mathrm{Re} = 2.67 \times 10^4$, and found through numerous numerical experiments that when the nondimensional time step, $\Delta t U/D$, is from 0.05 to 0.1, the

numerical diffusion is smaller than the physical diffusion and the computational error is acceptable. Thus in this paper we chose 0.075 as the optimal nondimensional time step for all the simulations. The procedure used to determine vortex–cylinder interaction at each time step can be divided into five steps as follows: (i) the vorticity field is determined using the SVM, and the unsteady fluid force coefficients are determined using Eqs. (4) and (5); (ii) the displacement and velocity of the structures are computed by a Runge–Kutta method using Eq. (6); (iii) the structures are moved according to their displacements, and the vorticity is changed accordingly; (iv) the strength of the surface vortices on the structure is changed under the influence of the velocity of the structure; (v) the modified vorticity distribution caused by the vibration of the structures will affect the fluid forces in the next time step. In such a process, the unsteady fluid forces, the structure vibrations, and the vorticity field are evaluated in an iterative way so that the interactions between the fluid and the structure are simulated properly.

At any instant, the cylinders are surrounded by a vorticity cloud with an infinite outer boundary of fluid medium. When the flexible cylinder moves under the action of the unsteady forces, the vortices contained within the fluid medium also move. The farther away the vortices are from the cylinder, the smaller the distance the vortices will move. A simplified model is proposed to describe this effect. The model assumes that the displacement of a vortex can be considered to be inversely proportional to the $n$th power of the vortex-to-structure distance. Therefore, if there is only one moving cylinder, the displacement of a vortex is determined by the displacement of the cylinder and the vortex-to-cylinder distance. If there are more than one moving cylinders, the displacement of a vortex is the sum of that caused by each moving cylinder, i.e.,

$$\mathbf{Z}_{Vj} = \sum_i \mathbf{Z}_{Ti} \frac{1}{d_{ij}^n}, \tag{7}$$

where $\mathbf{Z}_{Vj}$ are the displacements of the $j$th vortex, $\mathbf{Z}_{Ti}$ are the displacements of the $i$th structure, $d_{ij}$ is the distance between the $j$th vortex and the $i$th structure. Numerical experiments with $n$ in the range from 1 to 2 in steps of 0.2 indicated that the solution is not very sensitive to the choice in this range, therefore, $n$ is chosen to be unity in the present study.

For rigid cylinders in a uniform flow, the strength of the surface vortices is determined by Martensen's potential flow method, taking into account the additional coupling effects of free vortices. For flow-induced vibration of flexible cylinders, surface vortices on the cylinders are caused not only by the mainstream velocity $U$, but also by the motion of the cylinders. In order to calculate the surface vortex strength of the vibrating cylinders, another term has to be added to Eq. (2) to account for the motion of the cylinders. Therefore, if the mainstream direction is aligned with the $x$-direction (i.e., $\alpha = 0$), the strength of the $m$th surface vortex element in one of the cylinders can be deduced as

$$\sum_{n=1}^{M} \gamma(s_n) K(s_n, s_m) \Delta s_n = \left[ (-U + v_x) \frac{\mathrm{d}x_m}{\mathrm{d}s_m} \cos\alpha + v_y \frac{\mathrm{d}y_m}{\mathrm{d}s_m} \sin\alpha \right] + \sum_{i=1}^{I} \Delta\Gamma_i L(i,m), \tag{8}$$

where $v_x$ and $v_y$ are the vibration velocity of the cylinder in the $x$- and $y$-direction, respectively.

In the present simulation, two influencing factors are considered for the fluid–structure interaction process. One is the effect of tube displacement on the free vortices, Eq. (7), and the other is the tube velocity on the generation of surface vortices, Eq. (8). Eq. (7) is a simple model based on conservation of mass and free vortices in the fluid medium such that when the flexible cylinder moves under the action of the unsteady forces, the vortices contained within the fluid medium also move. In order to compare the sensitivity of these two factors, we had simulated flow-induced vibration of a single flexible cylinder regarding only the displacement of the tube and neglecting the velocity of the tube (denoted as the 'velocity-ignoring model' in Lam et al., 2004). The vibration amplitude and the fluctuation lift of the 'velocity ignoring model' in the lock-in region is much smaller than the experimental results. As pointed out by Lam et al. (2004), Eq. (8) has a greater effect than Eq. (7). Therefore, in comparison with the effect of the tube displacement on free vortices, the effect of tube velocity on vorticity generation is the main source of change of the fluid forces on the tube. Eqs. (7) and (8) were used in the simulation of the present study.

In general, the natural frequency of the tube, the frequency of the fluctuation lift for a vibrating tube and a stationary tube and the vortex shedding frequency have different physical meanings although they may take the same value. In our paper, the frequency of vortex shedding $f_s$ is actually obtained from the frequency of the lift coefficient $C_L$ in the calculation of flow across tube bundles. During the calculation, the mainstream velocity $U$ is chosen to be constant equal to 1 m/s, and the tube diameter $D$ is changed in proportion to the kinematic viscosity $v$ to fulfil the Re condition. At the given Re, $f_0$ is the frequency of $C_L$ of a single cylinder when the cylinder is not allowed to vibrate (rigid). After obtaining $f_0$, the value $\mathrm{St}^* = f_0 D/U$ is held constant and used in the calculation of $S_G = 8\pi^2 \mathrm{St}^{*2} M\zeta$, while $f_s$ is the shedding frequency of flow past a row of cylinders and its value is not known a priori. So for the tube bundle both rigid or flexible cylinders, we defined the nondimensional shedding frequency $\mathrm{St} = f_s D/U$ for our analysis. The natural

frequency of the tube $f_N$ is a variable related only with mass and stiffness of the tube. In order to study the FIV of the tube bundle, we change the $f_N/f_0$ ratio in the simulation by changing $f_N$ and keeping $f_0$ constant. The different values of $S_G = 8\pi^2 \mathrm{St}^{*2} M\zeta$ are simulated by changing the damping ratio $\zeta$ and mass ratio $M$.

## 3. Vortex-induced vibration of a row of cylinders

Fig. 1 shows the layout of a row of seven cylinders normal to the oncoming uniform flow $U$. It is well known that the initial flow behind a row of cylinders at small pitch ratio $T/D$ is highly nonuniform and is dominated by wide and narrow wakes. In order to examine the present model, the flow past a rigid cylinder row at pitch ratios $T/D = 1.5$ and 2.0 is first simulated. Once completed, the fluid–structure interaction of a flexible cylinder row at $T/D = 2.0$ at a lock-in situation is simulated to test the suitability of the SVM model for the simulation of cylinder arrays with large amplitude vibration. At small $T/D$, flow-induced vibration due to vortex shedding is suppressed, and fluidelastic instability becomes dominant. In order to validate the suitability of the SVM model for fluidelastic instability prediction of a cylinder row, the flow-induced vibration of a flexible cylinder row with different structural parameters at $T/D = 1.5$ is also simulated.

### 3.1. Flow behind a row of rigid cylinders

Zdravkovich (2003) systematically reviewed the work of flow past a row of rigid cylinders and pointed out that, for $T/D$ no less than 1.5, a narrow near-wake and a wide near-wake are formed. Fig. 2 shows the vorticity maps (the radius of the tiny circle in the figure represents the vorticity strength of each free vortex at a particular position, and the line crossing the radius represents the instantaneous velocity vector of each free vortex) of the flow past a single row of cylinders at two different $T/Ds$. It can be seen that the narrow near wake and the wide near wake are prominently reproduced in the vorticity map for $T/D = 1.5$ (Fig. 2(a)), while for $T/D = 2.0$ (Fig. 2(b)) the phenomenon becomes less significant. Strong jet-flow is formed between the cylinders (Fig. 2(a)).

Zdravkovich and Stonebanks (1990) studied experimentally the unsteady fluid force coefficients of four adjacent tubes in a single row of 11 cylinders at $T/D = 1.5$ with $\mathrm{Re} = 5.8 \times 10^4$ based on the mean gap velocity. The $\bar{C}_L$ of the four cylinders are 0.07, 0.00, 0.01 and 0.08, with a variation of $\pm 0.08$, while the $\bar{C}_D$ are 0.99, 0.75, 0.81, 0.37, with a variation of $\pm 0.07$. In the present calculation (results in Table 1), the $\bar{C}_L$ of the five adjacent cylinders in the centre of the single row at $T/D = 1.5$ vary from $-0.04$ to 0.05, while the $C'_L$ vary from 0.05 to 0.06. The $\bar{C}_D$ of the five adjacent cylinders in the centre of the single row vary from 0.35 to 0.54, and $C'_D$ range from 0.04 to 0.07. Compared with experimental results, the computational results are in reasonable agreement. The exceptions are the calculated $\bar{C}_D$ which are somehow lower than the experiment values. This suggests that in this case, besides the assumption of the 2-D calculation, the discrepancy between the unconfined flow condition in the present simulation and the blockage effects in the wind tunnel experiments is also an important reason for the differences between simulation and experimental results. But its effect on the centre part of the row of cylinders is still limited. So, simulating the FIV of the centre tubes

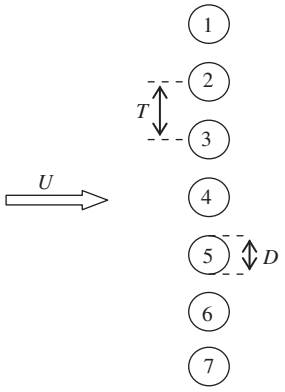


Fig. 1. Schematic layout of a cylinder row in a uniform flow.

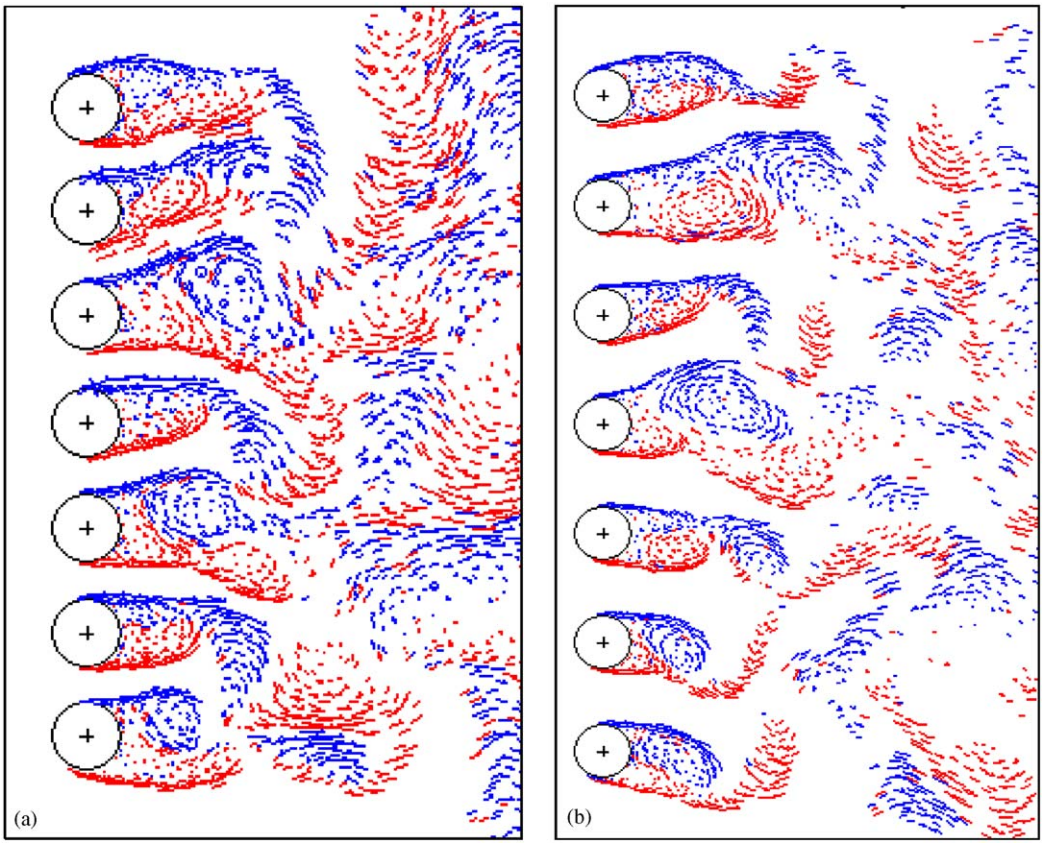


Fig. 2. Vorticity maps of the flow past a cylinder row; comparison of the simulation results at: (a) $T/D = 1.5$ and (b) $T/D = 2.0$. The radius of the tiny circle in the figure represents the vorticity strength of each free vortex, and the line crossing the radius represents the instantaneous velocity vector of each free vortex.

Table 1
Comparison of the fluid force coefficients and St of a row of rigid cylinders at different $T/D$s

| | Cylinder 2 | Cylinder 3 | Cylinder 4 | Cylinder 5 | Cylinder 6 |
|---|---|---|---|---|---|
| $T/D = 1.5$ | | | | | |
| $\bar{C}_L$ | 0.05 | −0.01 | −0.04 | −0.02 | −0.03 |
| $C'_L$ | 0.06 | 0.06 | 0.06 | 0.05 | 0.05 |
| $\bar{C}_D$ | 0.54 | 0.53 | 0.48 | 0.41 | 0.35 |
| $C'_D$ | 0.07 | 0.05 | 0.05 | 0.04 | 0.04 |
| St | | | 0.06, 0.27, 0.39 | | |
| $T/D = 2.0$ | | | | | |
| $\bar{C}_L$ | −0.06 | −0.03 | 0.01 | 0.04 | 0.02 |
| $C'_L$ | 0.10 | 0.11 | 0.10 | 0.11 | 0.11 |
| $\bar{C}_D$ | 0.45 | 0.46 | 0.39 | 0.48 | 0.52 |
| $C'_D$ | 0.06 | 0.05 | 0.03 | 0.04 | 0.04 |
| St | | | 0.20, 0.27 | | |

using an unconfined tube array by the SVM is still reasonable for engineering applications. It should be noted that since we did not put two wall panels on the sides of the cylinder row, the issue of pressure drop has not been addressed, especially when the number of rows of cylinders is large. However, most of the present simulations are on a single row

of cylinders. We expected the effect of pressure drop will not have great significance on our simulation. For example, if we focus our attention on the characteristics relative to the flow patterns in the tube gap we can see that the simulation results of the centre tubes in this unconfined tube array simulation and the experimental results of the centre tubes in the tube array in a finite duct have many similarities.

It is generally noted that the flow past a cylinder row at small $T/D$ gives rise to at least two shedding frequencies. Zdravkovich and Stonebanks (1990) conducted frequency measurements of a single row of cylinders of 11 cylinders at $T/D = 1.5$ and $\mathrm{Re} = 4.11 \times 10^4 - 4.90 \times 10^4$, and found three nondimensional shedding frequencies $\mathrm{St} = f_s D/U$, namely $\mathrm{St} = 0.05$, 0.28, and 0.40. In the present computation, these multiple frequency characteristics are also obtained. The St of the five centre cylinders varies between 0.06, 0.27 and 0.39 as listed in Table 1 and are in excellent agreement with experiments.

Table 1 shows the comparison of the fluid force coefficient and nondimensional shedding frequency St of the centre cylinders in a rigid cylinder row at different $T/D$s. The fluid force coefficients are based on the gap velocity $U_g = U(T/D)/(T/D - 1)$ for the sake of comparison, while St is based on the free-stream velocity $U$. It can be seen that with increasing $T/D$ (from 1.5 to 2.0), $C'_L$ of the five cylinders increases noticeably (from around 0.06 to 0.11), while $C'_D$ decreases only slightly (from 0.04–0.07 to 0.03–0.06). Compared with the results of $T/D = 1.5$, the calculated $\bar{C}_D$ at $T/D = 2.0$ is more uniform. This implies that the nonuniform phenomenon is less significant at $T/D = 2.0$ and flow-induced vibration due to vortex shedding is dominant. This conclusion is also supported by the calculated St at two different $T/D$s; St at $T/D = 2.0$ is reduced from three widely different values (0.06, 0.27, and 0.39) to two relatively similar values (0.20 and 0.27). These latter values are close to the St of a single cylinder (0.22) obtained by SVM at similar Re (Lam et al., 2004).

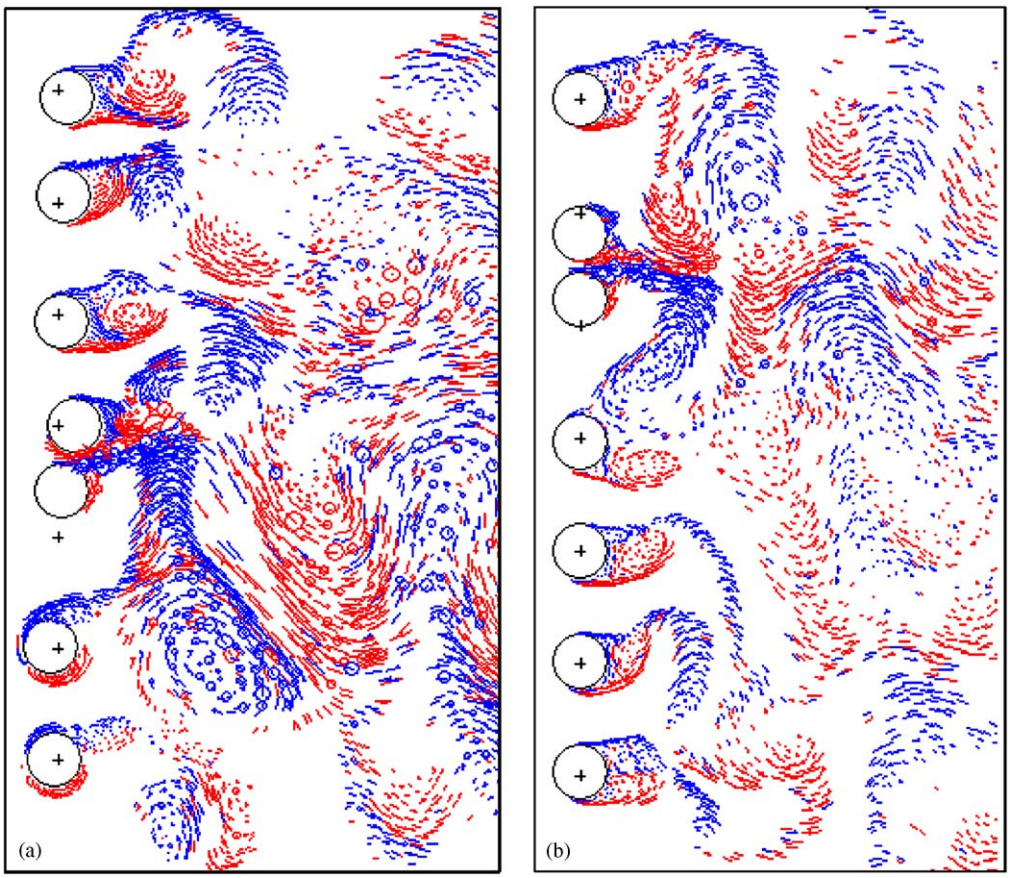


Fig. 3. Vorticity map of the flow past a flexible cylinder row with different degree-of-freedom models at $T/D = 2.0$ and $f_N/f_0 = 1.0$: (a) 2-dof model; and (b) 1-dof model.

### 3.2. Fluid–structure interaction of a fully flexible cylinder row at $T/D = 2.0$

The grid-free SVM is suitable for simulating FIV problems with large amplitude vibrations, because the cylinders can move freely over a large distance without the constraint of the grid. In this section, simulation of the fluid–structure interaction of a flexible cylinder row with FIV being dominated by vortex shedding is attempted. This phenomenon arises for $T/D = 2.0$. The computation is conducted at $f_N/f_0 = 0.5$ and 1.0, where $f_N$ is the cylinder natural frequency and $f_0$ is the shedding frequency of the flow past a rigid cylinder, $M = 10$, $\zeta = 0.0317$, and $S_G = 8\pi^2 \mathrm{St}^{*2} M\zeta = 1.29$ is the reduced damping parameter, which is similar to the definition adopted by Zhou et al. (1999), Liu et al. (2001) for convenience of comparison of simulation results.

The case at $f_N/f_0 = 1.0$ is considered first. Figs. 3(a) and (b) show, respectively, the vorticity map of the flow-induced vibration of the cylinder row with a 2-dof and a 1-dof model assumed. As expected, the vibration amplitude of some of the cylinders is very large. Frequency analysis shows that the vortex shedding frequency and cylinder vibration frequency of the vibrating cylinder row are close to the cylinder natural frequency, i.e., close to the lock-in region. The vorticity clouds are formed behind the large-amplitude oscillating cylinders, and the wake flow of the cylinder row is changing dramatically compared with that of the rigid cylinder row. A jet flow occurs when two of the cylinders approach each other. This is the case irrespective of whether the vibration model assumed is a 1-dof or a 2-dof model. The vorticity map of the cylinder row with a 2-dof model assumed (Fig. 3(a)) is more irregular than that of the cylinder row with a 1-dof model (Fig. 3(b)).

The locus of the cylinder centre of the vibrating cylinders with a 2-dof model assumed is shown in Fig. 4. On the other hand, the vibration response time history of the seven cylinders assuming a 1-dof model is plotted in Fig. 5. In Fig. 4 the vibration responses of the cylinders in the $x$ direction are larger than that in the $y$ direction except for cylinder 5, where the maximum vibration response occurs in the $y$ direction and the amplitude is about $0.85D$. This compares to maximum vibration amplitude of $0.52D$ in cylinder 3 for the 1-dof model calculation (Fig. 5).

Through comparison of the vorticity map and the vibration amplitude of the 1-dof and 2-dof model calculation of the cylinder row, it could be concluded that the crosstalk between the $x$- and $y$-direction vibration is not negligible for large-amplitude vibration. The same behaviour is also observed in the calculated $C'_L$ for the case $f_N/f_0 = 1.0$ (Table 2). The 2-dof model yields a $\bar{C}_L$ range of $-0.15$–$0.08$, and a $C'_L$ variation of 0.26–0.55. The corresponding variations are $-0.07$–$0.02$ for $\bar{C}_L$ and 0.14–0.47 for $C'_L$ when the 1-dof model was invoked.

These results led to an important question. If the vibration amplitude is small, does the vibration in the $x$ direction still have an important effect on the vibration response in the $y$ direction for a row of freely vibrating cylinders? In order to answer this question, a simulation at $f_N/f_0 = 0.5$ was carried out. The fluctuating forces are very small. For example, $\bar{C}_L$ varies around $0 \pm 0.02$, while $C'_L$ hovers between 0.10 and 0.12 for the 2-dof and 1-dof model calculations (Table 2). This implies that the vibration amplitude is also very small because the forcing function in Eq. (6) is small. The vorticity maps of the cylinder row are quite similar to those of a rigid cylinder row. These results suggest that for small-amplitude vibration, the crosstalk between the $x$- and $y$-direction could be neglected, and the 1-dof model can be used to account for flow-induced vibration of a cylinder row. This realization is important for cylinder array simulation because it greatly simplifies the calculations for multiple and complex arrays.

### 3.3. Fluid–structure interaction and fluidelastic instability of a fully flexible cylinder row at $T/D = 1.5$

An array of cylinders placed in a uniform flow may undergo instability beyond a certain threshold flow velocity. At small $T/D$, flow-induced vibration due to vortex shedding is suppressed by the relatively smaller gap between the cylinders, and fluidelastic instability behaviour becomes dominant. In this section, the flow-induced vibration due to fluidelastic instability of a single cylinder row is discussed. The computation is carried out at $T/D = 1.5$, $M = 10$ and 50, $\zeta = 0.0317$, and $f_N/f_0 = 1.0$–$4.46$. Altogether, three cases characterized by their mass ratio and their rigidity are considered and they are: case 1 with small mass ratio and large rigidity ($S_G = 1.29$, $M = 10, f_N/f_0 = 2.98$); case 2 with small mass ratio and smaller rigidity ($S_G = 1.29$, $M = 10, f_N/f_0 = 1.79$); case 3 with large mass ratio and more flexible ($S_G = 6.54$, $M = 50, f_N/f_0 = 1.00$). For small-gap flow with $T/D = 1.5$, the vibration amplitude of the cylinder row is small. Therefore, it is not necessary to assume a 2-dof model for the structural dynamics; a 1-dof model will suffice.

#### 3.3.1. Vorticity map

Fig. 6 shows the vorticity map for the three cases studied: Fig. 6(a) is for case 1; Fig. 6(b) is for case 2; and Fig. 6(c) is for case 3. It can be seen from the wake flow of case 2 (Fig. 6(b)) that the vibration of the cylinders is more violent than that shown for case 1 (Fig. 6(a)) and case 3 (Fig. 6(c)). At $M = 10$ (case 1 and 2), with a decrease in the natural frequency, the oscillation of the cylinders increases, and the vibrating cylinders interact with the flow and cause a

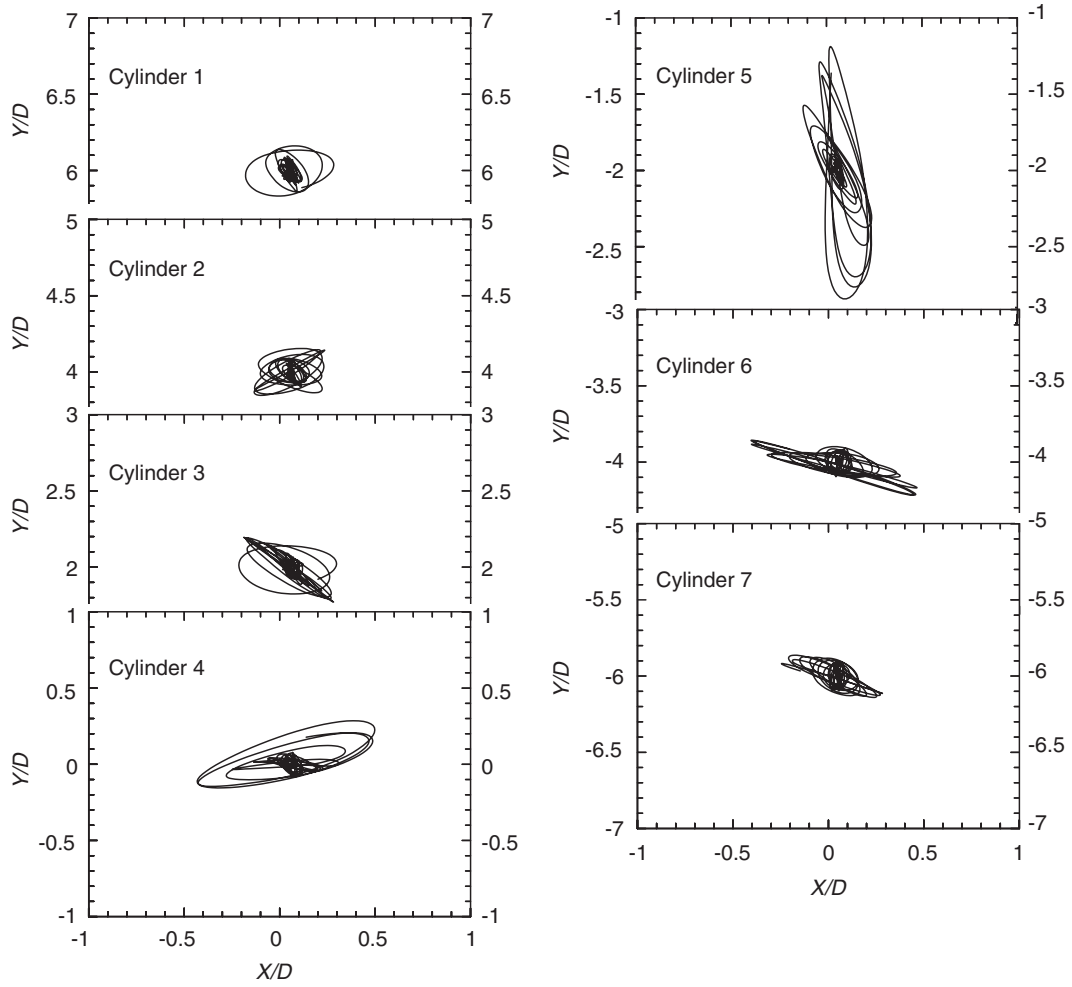


Fig. 4. Locus of the vibrating cylinders ($f_N/f_0 = 1.0$, $S_G = 1.29$) in a cylinder row with $T/D = 2.0$ with datum for $y$ at centre of cylinder 4.

dramatic change in the vorticity field. At $M = 50$ (case 3), although the natural frequency of cylinders is lower and is chosen to be equal to the shedding frequency of a rigid cylinder, the vorticity map is still more orderly than that shown for the case 2 where $M = 10$ and $f_N/f_0 = 1.79$ due to the very high $S_G$ value used in the simulation.

### 3.3.2. *Vibration response*

The time histories of the vibration response of the flexible cylinder row for case 1, 2 and 3 are shown in Figs. 7–9, respectively. For case 1 where $M = 10$ and $f_N/f_0 = 2.98$ (Fig. 7), the maximum vibration amplitude is $0.011D$ and occurs at cylinders 2 and 3, the r.m.s. vibration response of the cylinders is small, ranging from $0.001D$ to $0.003D$. The multiple frequency characteristics are distinctive in the vibration response, and the primary response frequencies of the cylinders are high. For case 2 ($M = 10$ and $f_N/f_0 = 1.79$), the maximum vibration amplitude is $0.287D$ and occurs at cylinder 2 (Fig. 8), the r.m.s. vibration responses of the cylinders are large, ranging from $0.026D$ to $0.125D$. The primary response frequencies are not as high as those deduced for case 1 due to the change of wake size when more significant fluid–structure interaction occurs as $f_N$ approaches $f_0$. The vibration response frequencies of the cylinders are monotonic. For case 3 ($M = 50$ and $f_N/f_0 = 1.00$), the maximum vibration amplitude is $0.034D$ and occurs at cylinder 1 (Fig. 9), the r.m.s. vibration responses of the cylinders are still relatively small, ranging from $0.006D$ to $0.013D$. Multiple frequency characteristics are evident in the vibration response. The primary response frequencies of the cylinders are lower than those discerned in Fig. 8.

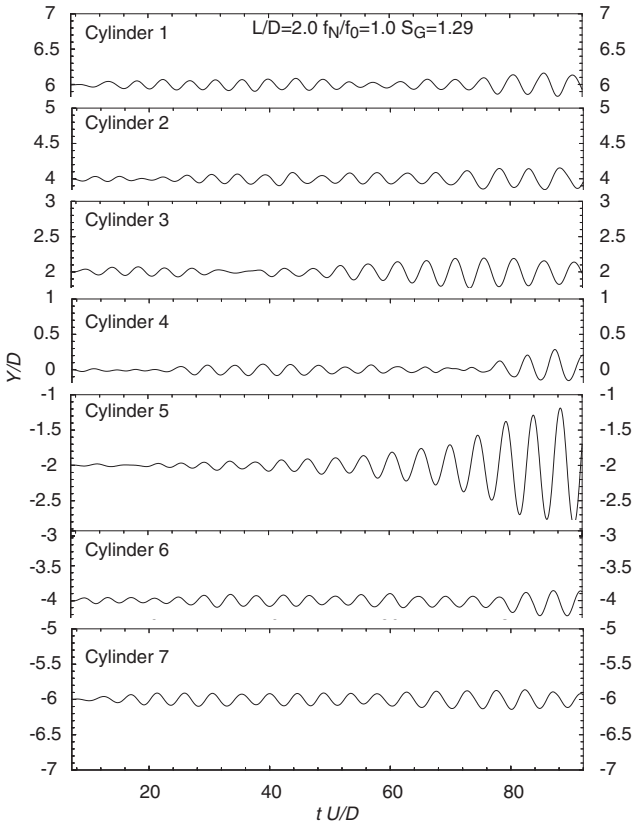


Fig. 5. Vibration response time history of a row of seven cylinders ($T/D = 2.0$) calculating using a 1-dof model with $f_N/f_0 = 1.0$ and $S_G = 1.29$.

Table 2
The lift force coefficient of a cylinder row calculated with 1- and 2-dof models and different flexibility at $T/D = 2.0$

| | | Cylinder 2 | Cylinder 3 | Cylinder 4 | Cylinder 5 | Cylinder 6 |
|---|---|---|---|---|---|---|
| $f_N/f_0 = 1.0$ | | | | | | |
| 2-dof model | $\bar{C}_L$ | −0.02 | −0.02 | 0.08 | 0.02 | −0.15 |
| | $C'_L$ | 0.29 | 0.26 | 0.38 | 0.55 | 0.39 |
| 1-dof model | $\bar{C}_L$ | 0.02 | −0.07 | −0.03 | −0.02 | −0.01 |
| | $C'_L$ | 0.39 | 0.47 | 0.33 | 0.14 | 0.18 |
| $f_N/f_0 = 0.5$ | | | | | | |
| 2-dof model | $\bar{C}_L$ | −0.03 | −0.03 | −0.05 | 0.00 | 0.02 |
| | $C'_L$ | 0.11 | 0.12 | 0.11 | 0.11 | 0.10 |
| 1-dof model | $\bar{C}_L$ | −0.03 | −0.04 | −0.02 | −0.04 | −0.05 |
| | $C'_L$ | 0.11 | 0.11 | 0.11 | 0.12 | 0.11 |

### 3.3.3. Fluid force

The mean and r.m.s. lift coefficients of each cylinder in cases 1, 2 and 3 are tabulated in Table 3. Variations of $\bar{C}_L$ of the cylinders are about 0.10, and are almost the same as those shown in Table 1 for the rigid cylinder row. The $C'_L$ of the cylinders in case 2 ($M = 10$ and $f_N/f_0 = 1.79$) range from 0.20 to 0.27, and are much higher than those calculated for the other two cases. For cases 1 and 3, $C'_L$ varies from 0.04 to 0.07 and from 0.05 to 0.06, respectively, and these values are close to those given in Table 1 (0.05–0.06) for a rigid cylinder row.

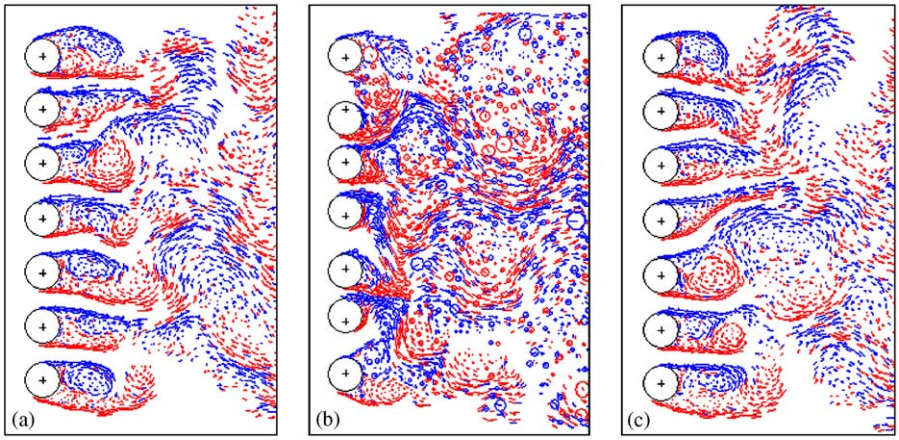


Fig. 6. Vorticity map of the flow past flexible cylinders in a row with $T/D = 1.5$ for three cases with different structural parameters: (a) case 1 with $S_G = 1.29$, $M = 10$, $f_N/f_0 = 2.98$; (b) case 2 with $S_G = 1.29$, $M = 10$, $f_N/f_0 = 1.79$; and (c) case 3 with $S_G = 6.54$, $M = 50$, $f_N/f_0 = 1.00$.

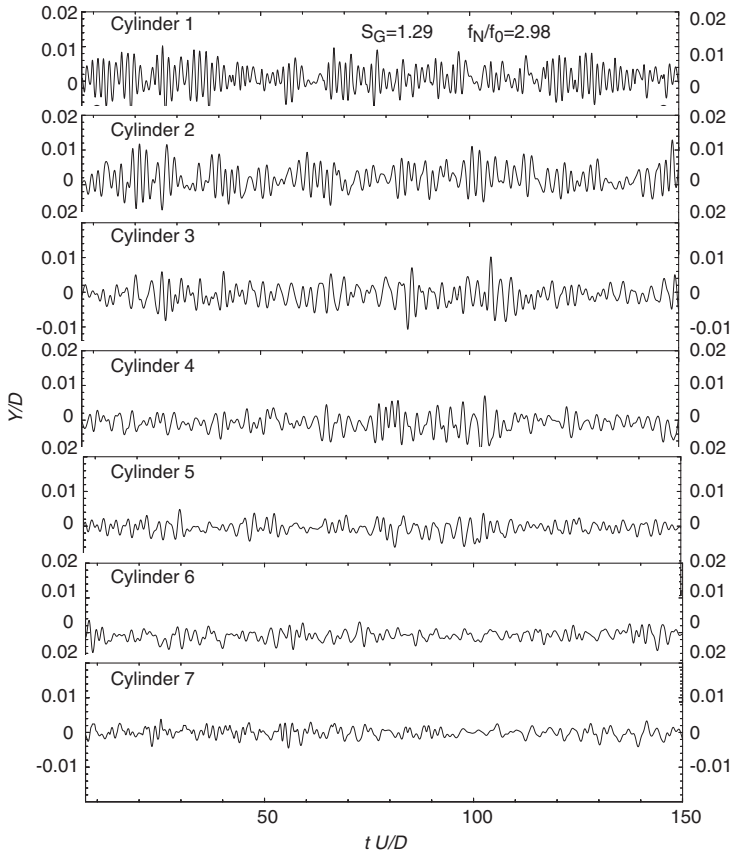


Fig. 7. Time history of the flow-induced vibration of a flexible cylinder row for case 1 where $S_G = 1.29$ and $f_N/f_0 = 2.98$.

### 3.3.4. Fluidelastic instability

Cylinders 2–6 in the centre of the cylinder row can be used to approximate the middle portion of an infinite cylinder row. The r.m.s. value of the $y$-direction vibration amplitude $(Y/D)_{\text{r.m.s.}}$ and frequency of the flow-induced vibration

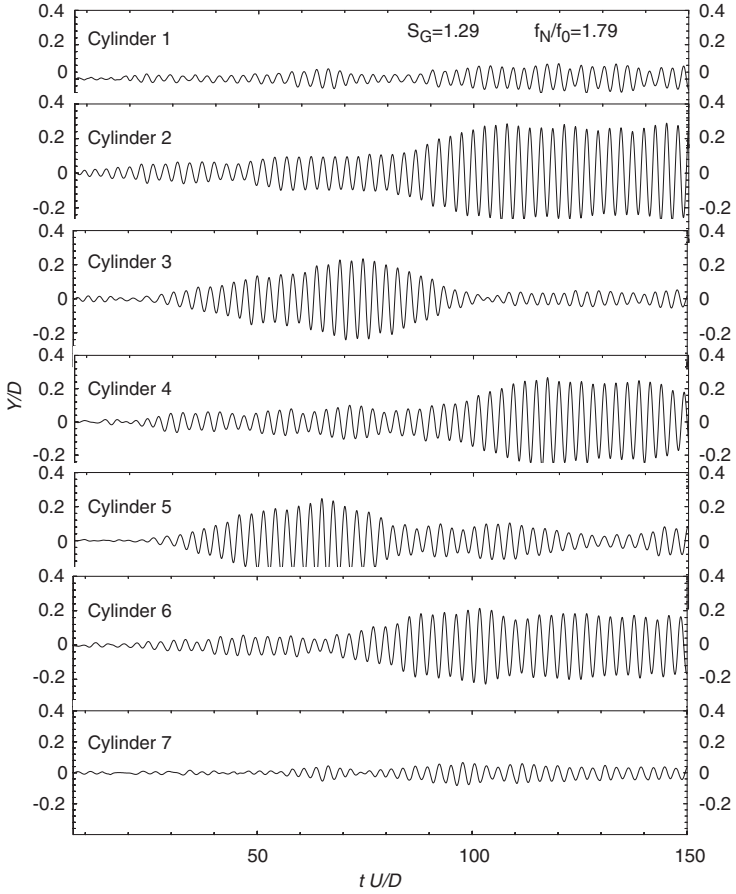


Fig. 8. Time history of the flow-induced vibration of a flexible cylinder row for case 2 where $S_G = 1.29$ and $f_N/f_0 = 1.79$.

response of the five cylinders at $S_G = 1.29$ are shown versus the reduced flow velocity in Figs. 10 and 11, respectively. In order to compare with experimental data, the reduced flow velocity is based on the gap flow velocity. In the simulation, the variation of the reduced velocity $U_{rg} = U_g/(f_N D)$ is obtained by changing the natural frequency $f_N$. It can be seen that at $U_{rg} = 3.0$ and 4.5, $(Y/D)_{\text{r.m.s.}}$ of the five cylinders are very small, and multiple frequencies occur in the vibration response. The largest response is at the tube natural frequency. From $U_{rg} = 4.5$ to 6.0, $(Y/D)_{\text{r.m.s.}}$ increases, while the increase is rather rapid from $U_{rg} = 6.0$ to 6.69 then to 7.5. At $U_{rg} = 6.0$, 6.69 and 7.5, the vibration frequency, which is a little smaller than the natural frequency, is distinctly visible for the vibrating cylinders. The critical $U_{rg}$ stands at about 6.0 for $S_G = 1.29$.

The present critical $U_{rg}$ is plotted in Fig. 12 together with the experimental results of a multi-flexible single row of cylinders compiled by Price (1995) and the analytical results of a single row of cylinders with $T/D = 1.33$ using the unsteady model (Tanaka et al., 2002). It can be observed that the present model reasonably estimated the fluidelastic instability boundary for $S_G = 1.29$. The simulation result with $M = 50$ and $f_N/f_0 = 1.00$ corresponding to $S_G = 6.45$ and $U_{rg} = 13.38$ is located within the stable steady region in Fig. 12, which is also demonstrated by its small-vibration amplitude.

## 4. Vortex-induced vibration of a staggered cylinder array

### 4.1. Simulation results of the SVM

The flow around several rows of cylinder array is far more complex especially when the cylinders are flexible. In this section, a simulation of the flow past a staggered cylinder array ($T/D = P/D = 2.0$) of three rows with five or four

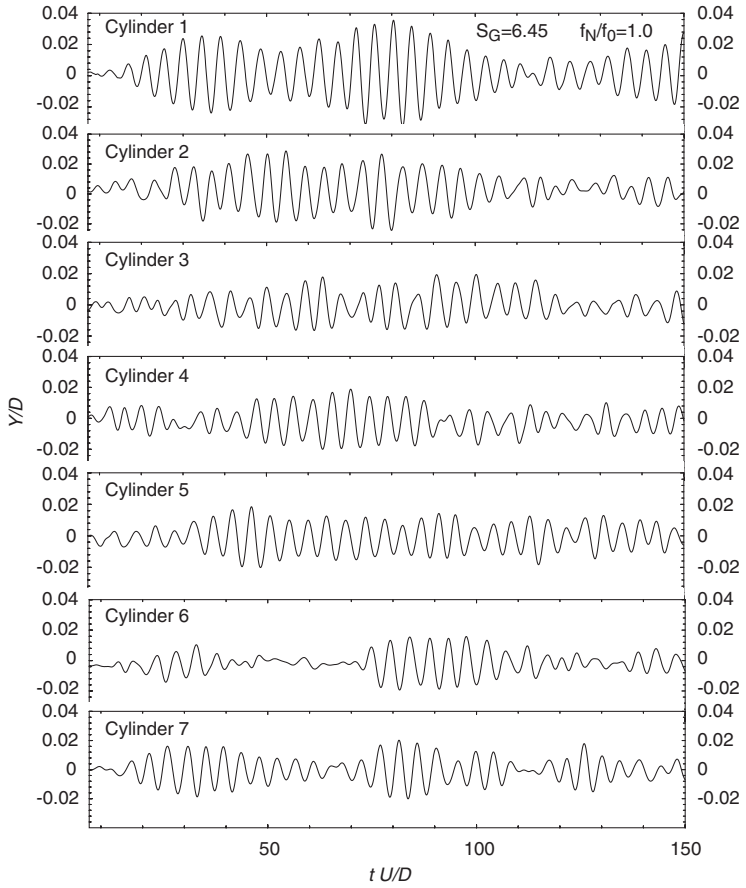


Fig. 9. Time history of the flow-induced vibration of a flexible cylinder row for case 3 where $S_G = 6.45$ and $f_N/f_0 = 1.00$.

Table 3
The lift force coefficients of the vibrating cylinder row with different structural parameters at $T/D = 1.5$

| Case | | | Cylinder 2 | Cylinder 3 | Cylinder 4 | Cylinder 5 | Cylinder 6 |
|---|---|---|---|---|---|---|---|
| 1 | $S_G = 1.29, f_N/f_0 = 2.98$ | $\bar{C}_L$ | 0.07 | −0.03 | −0.03 | −0.02 | −0.03 |
| | | $C'_L$ | 0.07 | 0.07 | 0.06 | 0.04 | 0.04 |
| 2 | $S_G = 1.29, f_N/f_0 = 1.79$ | $\bar{C}_L$ | 0.04 | −0.02 | −0.01 | −0.03 | −0.06 |
| | | $C'_L$ | 0.27 | 0.20 | 0.24 | 0.22 | 0.26 |
| 3 | $S_G = 6.45, f_N/f_0 = 1.00$ | $\bar{C}_L$ | 0.06 | −0.01 | −0.05 | −0.02 | −0.04 |
| | | $C'_L$ | 0.06 | 0.07 | 0.06 | 0.05 | 0.05 |

cylinders in each row is attempted. Here, $P$ is the centre-to-centre distance between two rows of cylinders. The simulation is carried out for rigid cylinders as well as for flexible cylinders free to vibrate only in the $y$ direction with $S_G = 1.29, f_N/f_0 = 1.0$ and 2.0. This means that a 1-dof model is assumed for the cylinder dynamics.

Fig. 13 shows a comparison of the vorticity maps deduced from arrays having different structural parameters. It can be seen that when the cylinders are rigid, the flow around the cylinders is more orderly (Fig. 13(a)). The wake of the first row of cylinders is narrowed, while the hook-like wake of the second row of cylinders is wide, and in the last row, an alternate wide and narrow near-wake is formed. The flow pattern in the first and second row, especially the first row, is similar to the flow visualization results for normal triangular cylinder array with $P/D = 2.08$ and $\mathrm{Re} = 10\,000$ of

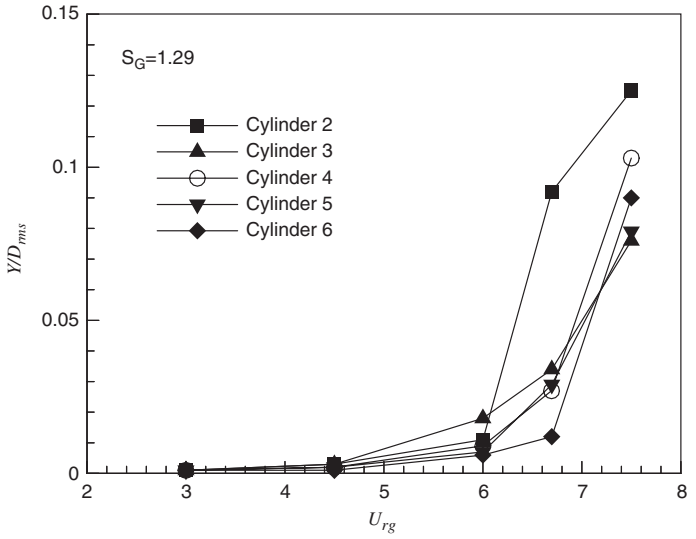


Fig. 10. The distribution of $(Y/D)_{\text{r.m.s.}}$ versus $U_{rg}$ for the flow past a flexible cylinder row at $T/D = 1.5$.

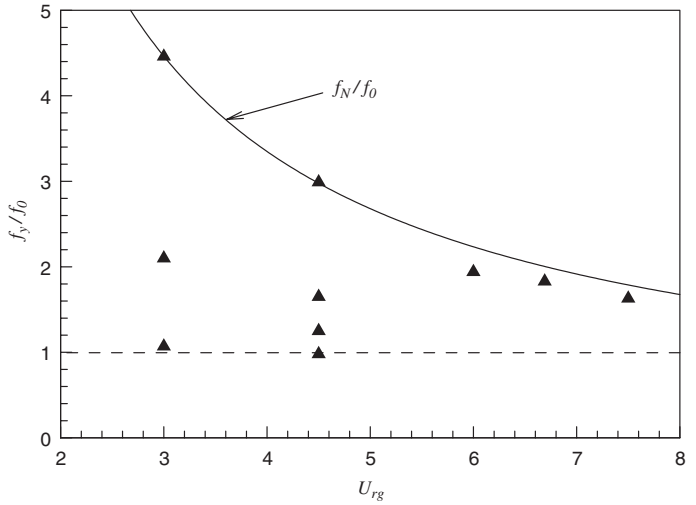


Fig. 11. The distribution of $f_y/f_0$ versus $U_{rg}$ for the flow past a flexible cylinder row at $T/D = 1.5$.

Oengoren and Ziada (1998) (in their Fig. 14f). The force frequency analysis of the cylinders in different rows is consistent with the vorticity distribution, i.e., the narrow wake of the first row corresponds to a higher nondimensional vortex shedding frequency of 0.26, the wide wake of the second row to 0.17, while the third row has multiple frequencies of 0.26 and 0.12. We compare the frequency analysis results with the experimental results of Oengoren and Ziada (1998) of flow past normal triangular tube array with $P/D = 2.08$ and $\text{Re} = 26\,300$. Their measurements showed that two frequencies are clearly visible in the first row with the higher frequency is dominant, and in the second row two shedding frequencies and their difference frequency are shown, while in the further six rows only the first row domain frequency and the difference frequency exist. The discrepancy in the behaviour may be due to the fact that Oengoren and Ziada considered a 14-row array, while this paper simulates a three-row array in unconfined flow.

The vorticity map of the flexible cylinder array at $f_N/f_0 = 2.0$ is slightly more irregular than that of the rigid cylinders, but the whole flow pattern is similar. The vibration amplitude is quite small (Fig. 14), the maximum vibration amplitude of $0.06D$ occurs at cylinder 11 in the third row, and the vibration response increases along the streamwise

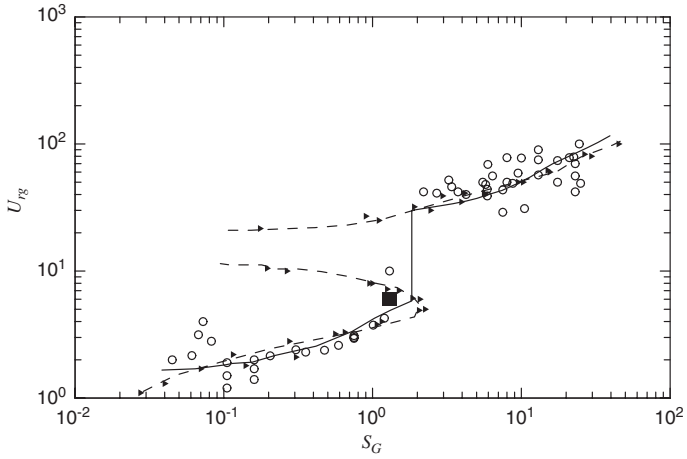


Fig. 12. Critical $U_r$ for a single row of flexible cylinders versus $S_G$: (○) experimental results compiled by Price (1995); (—) practical stability standard; (–►–) analytical results of Tanaka et al. (2002) for a single row of cylinders at $T/D = 1.33$; and (■) present calculations.

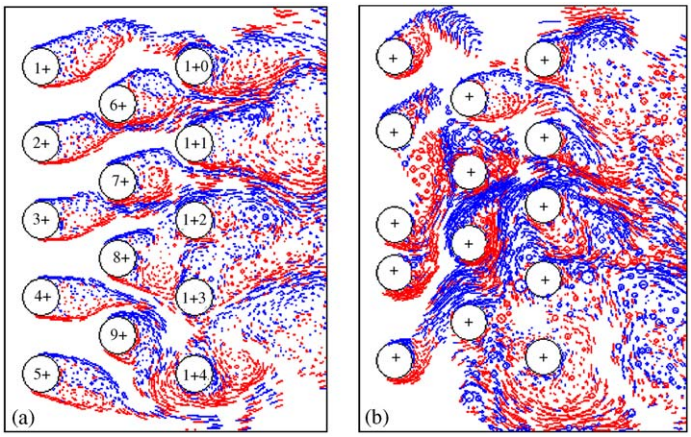


Fig. 13. Vorticity map of the flow past a staggered cylinder array $T/D = P/D = 2.0$: (a) rigid cylinders; and (b) flexible cylinders with $S_G = 1.29$ and $f_N/f_0 = 1.0$.

direction. The vorticity map for the flexible cylinder array at $f_N/f_0 = 1.0$ (Fig. 13(b)) is quite different from that of the rigid cylinders. Due to a large amplitude vibration in the first row (Fig. 15), jet flow occurs between cylinder 3 and 4, and the flow past the cylinder array changes violently. Contrast this to the situation where $f_N/f_0 = 2.0$, the vibration response of the cylinders decreases along the streamwise direction, and a maximum vibration amplitude of $0.69D$ occurs at cylinder 3 in the first row. The shedding frequency is between 0.22 and 0.26.

Comparing the vibration response of the two cases considered above, it is observed that in small-amplitude vibration the fluid–structure interaction is weak, the influence of cylinder vibrations on the flow field can be neglected, while in large-amplitude vibration, the fluid–structure interaction is strong, and the influence of cylinder vibration on the flow field is very significant.

We have spent a lot of effort to simulate the flow-induced vibration of multi-cylinder arrays using the finite element method (FEM), similar to Liu et al. (2001). Since there are so many bottlenecks involved in simulating the flow around multi-cylinders by grid-based methods, such as boundary layer solving, choice of turbulence model, grid formation and deformation, etc., we did not obtain good results compared to SVM. It is evident that FEM simulation is a very time-consuming and difficult approach compared to the SVM. For example, using SVM it only takes about 48 h of computational time in a Pentium 4 (CPU 1.7 GHz and 512 M RAM) to simulate flow-induced vibration of a staggered cylinder array with $S_G = 1.29$ and $f_N/f_0 = 1.0$, while our FEM simulation of a similar case failed after 10 days of computation. Using FEM, the vibration amplitude of the cylinders is constrained by the deformation of the meshes.

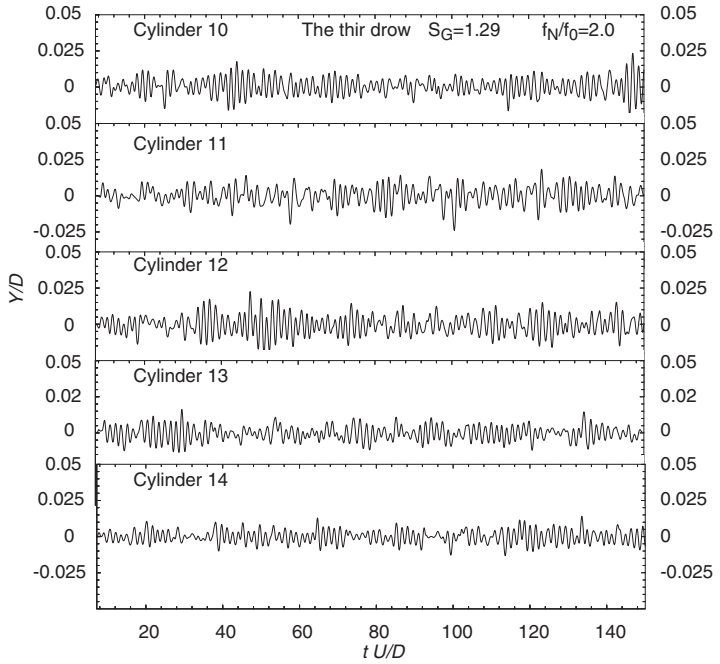


Fig. 14. Vortex-induced vibration of the third row of a staggered cylinder array at $f_N/f_0 = 2.0$.

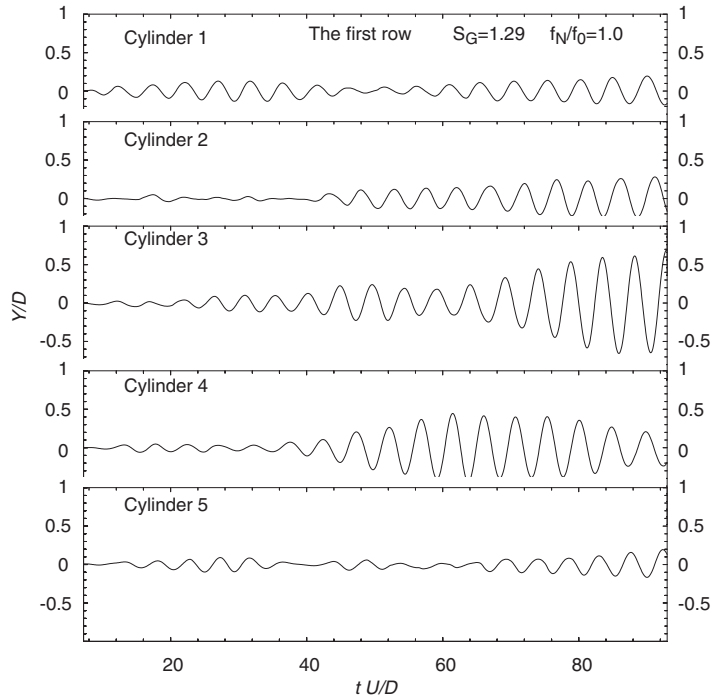


Fig. 15. Vortex-induced vibration of the first row of a staggered cylinder array at $f_N/f_0 = 1.0$.

Once the motion of a cylinder in a time step becomes too large, which would lead to mesh entanglement, computation breakdown would occur. On the other hand, using SVM the vibration amplitude of the cylinder can be as large as the problem allows, provided the cylinders do not coalesce with each other.

## 5. Conclusions

The flow-induced vibration of a single cylinder row and a staggered cylinder array are simulated by a fluid–structure interaction model based on the surface vorticity method (SVM) at a Reynolds number $\mathrm{Re} = 2.67 \times 10^4$, and the following conclusions can be made:

(1) The nonuniform flow behind a rigid cylinder row with a small pitch ratio $T/D = 1.5$, characterized by narrow and wide near wake and multiple frequencies, are replicated reasonably well by the SVM. The vortex shedding behind a rigid cylinder row with $T/D = 2.0$ is also reproduced.
(2) SVM is suitable for large-amplitude vortex-induced vibration simulation. The large-amplitude vibration of a cylinder row with $T/D = 2.0$ is calculated. It is found that the vorticity map and the fluid forces of the cylinder row change dramatically, and the $x$-direction vibration has a significant effect on the $y$-direction vibration. This rather significant crosstalk is absent in small-amplitude vibration cases. Therefore, the influence of the $x$-direction vibration on the $y$-direction can be neglected and a 1-dof structural dynamics model can be assumed to analyse the small amplitude vibration characteristics of the cylinder arrays.
(3) The FIV and fluidelastic instability of a flexible cylinder row with $T/D = 1.5$ is also studied. Simulations have been carried out for three cases where the structural parameters are quite different. The calculated vorticity map, vibration response, and fluid force of three cases are compared. The critical reduced velocity of the cylinder row at $S_G = 1.29$ is calculated. A comparison with experimental and analytical results shows that the present method reasonably estimates the fluidelastic stability threshold for $S_G = 1.29$. Furthermore, the simulation result shows that the small-amplitude vibration with $M = 50$ and $f_N/f_0 = 1.00$ is located in the stable region.
(4) Flow-induced vibration of a staggered cylinder array with $T/D = P/D = 2.0$ is simulated assuming different structural parameters. The vorticity map of the rigid cylinder array is compared with flow visualization results, and the basic flow characteristics are produced. The shedding frequency in the first row is higher than that calculated for the second row; this result is consistent with experimental data. When the cylinders become more flexible, the flow pattern changes drastically and fluid–structure interaction has a dominant impact on the flow. The results further show that, with a decrease of cylinder natural frequency, the maximum vibration response moves from the third row to the first row.
(5) Compared with grid-based methods, the grid-free SVM is an efficient and practical method for the simulation of the FIV of cylinder arrays at sub-critical Reynolds numbers.

## Acknowledgements

The authors wish to thank the Research Grants Council of the Hong Kong Special Administrative Region, China, for its support through Grant no. PolyU 5163/01E.

## References

Blevins, R.D., 1994. Flow-Induced Vibrations, second ed. Krieger, Florida.

Chen, S.S., Srikantiah, G.S., 2002. Motion-dependent fluid force coefficients for tube arrays in Crossflow. ASME Journal of Pressure Vessel Technology 123, 429–436.

Cottet, G.-H., Koumoutsakos, P., 2000. Vortex Method: Theory and Practice. Cambridge University Press, Cambridge.

Ichioka, T., Kawata, Y., Nakamura, T., Izumi, H., Nakamura, T., Fujita, K., 1994. Two-dimensional flow analysis of fluid structure interaction around a cylinder and a row of cylinders. In: Proceedings of the ASME Symposium on Flow-Induced Vibrations PVP-273, Minneapolis, USA, pp. 33–41.

Kassera, V., Strohmeier, K., 1997. Simulation of tube bundle vibrations induced by cross-flow. Journal of Fluids and Structures 11, 909–928.

Kevlahan, N., Ghidaglia, J.M., 2001. Computation of turbulent flow past an array of cylinders using a spectral method with Brinkman penalization. European Journal of Mechanics B 20, 333–350.

Lam, K., Jiang, G.D., Liu, Y., So, R.M.C., 2004. Grid-free surface vorticity method applied to flow induced vibration of flexible cylinders. International Journal for Numerical Methods in Fluids 46, 289–313.

Lewis, R.I., 1981. Surface vorticity modeling of separated flows from two-dimensional bluff bodies of arbitrary shape. Journal Mechanical Engineering Science 23, 1–12.

Lewis, R.I., 1991. Vortex Element Methods for Fluid Dynamic Analysis of Engineering System. Cambridge University Press, Cambridge.

Liu, Y., So, R.M.C., Lau, Y.L., Zhou, Y., 2001. Numerical studies of two side-by-side elastic cylinders in a cross-flow. Journal of Fluids and Structures 15, 1009–1030.

Longatte, E., Bendjeddou, Souli, M., 2003. Method for numerical study of tube bundle vibrations in cross-flow. Journal of Fluids and Structures 18, 513–528.

Mittal, S., Kumar, V., 2001. Flow-induced oscillations of two cylinders in tandem and staggered arrangements. Journal of Fluids and Structures 15, 717–736.

Moretti, P.M., 1993. Flow-induced vibrations in arrays of cylinders. Annual Review of Fluid Mechanics 25, 99–114.

Oengoren, A., Ziada, S., 1998. An in-depth study of vortex shedding acoustic resonance and turbulent forces in normal triangular tube arrays. Journal of Fluids and Structures 12, 717–758.

Ogami, Y., Akamatsu, T., 1991. Viscous flow simulation using the discrete vortex method—the diffusion velocity method. Computers and Fluids 9, 433–441.

Pettigrew, M.J., Taylor, C.E., 2003a. Vibration analysis of shell-and-tube heat exchangers: an overview—Part 1: flow, damping, fluidelastic instability. Journal of Fluids and Structures 18, 469–483.

Pettigrew, M.J., Taylor, C.E., 2003b. Vibration analysis of shell-and-tube heat exchangers: an overview—Part 2: flow, vibration response, fretting-wear, guidelines. Journal of Fluids and Structures 18, 485–500.

Païdoussis, M.P., 1983. A review of flow-induced vibrations in reactor and reactor components. Nuclear Engineering and Design 74, 31–60.

Price, S.J., 1995. A review of theoretical models for fluid-elastic instability of tubes in cross-flow. Journal of Fluids and Structures 9, 463–518.

Schroder, K., Gelbe, H., 1999. Two- and three-dimensional CFD-simulation of flow-induced vibration excitation in tube bundles. Chemical Engineering and Processing 38, 621–629.

Seitanis, S., Anagnostopoulos, P., 2000. Numerical study of the in-line oscillations of tube bundles. In: Ziada, S., Staubli, T. (Eds.), Proceedings of the Seventh International Conference on Flow Induced Vibrations, Lucerne, Switzerland, pp. 273–280.

Shiels, D., Leonard, A., Roshko, A., 2001. Flow-induced vibration of a circular cylinder at limiting structural parameters. Journal of Fluids and Structures 15, 3–21.

So, R.M.C., Liu, Y., Lai, Y.G., 2003. Mesh shape preservation for flow-induced vibration problems. Journal of Fluids and Structures 18, 287–304.

Sweeney, C., Meskell, C., 2003. Fast numerical simulation of vortex shedding in tube arrays using a discrete vortex method. Journal of Fluids and Structures 18, 501–512.

Tanaka, H., Tanaka, K., Shimizu, F., 2002. Fluidelastic analysis of tube bundle vibration in cross-flow. Journal of Fluids and Structures 16, 93–112.

Weaver, D.S., Fiztpatrick, J.A., 1988. A review of cross-flow induced vibrations in heat exchanger tube arrays. Journal of Fluids and Structures 2, 73–93.

Zdravkovich, M.M., 2003. Flow Around Circular Cylinders—A Comprehensive Guide Through Flow Phenomena, Experiments, Applications, Mathematical Models, and Computer Simulations, vol. 2. Oxford University Press Inc., New York.

Zdravkovich, M.M., Stonebanks, K.L., 1990. Intrinsically nonuniform and metastable flow in and behind tube arrays. Journal of Fluids and Structures 4, 305–319.

Zhou, C.Y., So, R.M.C., Lam, K., 1999. Vortex-induced vibrations of an elastic circular cylinder. Journal of Fluids and Structures 13, 165–189.